This is an open access article published under an ACS AuthorChoice License, which permits copying and redistribution of the article or any adaptations for non-commercial purposes.

ACS APPLIED MATERIALS & INTERFACES

Research Article

Cite This: ACS Appl. Mater. Interfaces 2018, 10, 33693−33706

www.acsami.org

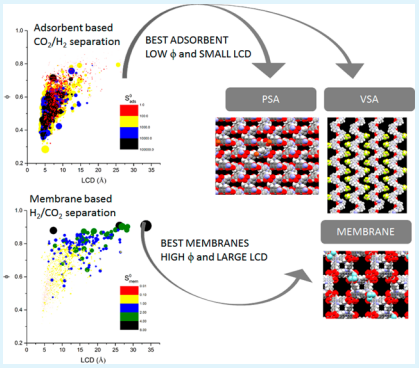
High-Throughput Screening of MOF Adsorbents and Membranes for H_2 Purification and CO_2 Capture

Gokay Avci, Sadiye Velioglu, and Seda Keskin*

Department of Chemical and Biological Engineering, Koc University, Rumelifeneri Yolu, Sariyer, 34450 Istanbul, Turkey

Supporting Information

ABSTRACT: Metal organic frameworks (MOFs) have emerged as great adsorbent and membrane candidates for separation of CO_2/H_2 mixtures. The main challenge is the existence of thousands of MOFs, which requires computational screening methods to identify the best materials prior to experimental efforts. In this study, we performed high-throughput computational screening of MOFs to examine their adsorbent and membrane performances for CO_2/H_2 separation. Grand canonical Monte Carlo (GCMC) and molecular dynamics (MD) simulations were used to compute various adsorbent and membrane performance metrics of 3857 MOFs. CO_2/H_2 adsorption selectivities of MOFs at pressure swing adsorption (PSA) and vacuum swing adsorption (VSA) conditions were calculated to be in the range of 2.5−25 000 and 2.5−85 000, respectively, outperforming many zeolite adsorbents. Correlations between the ranking of MOF adsorbents at the PSA and VSA conditions were examined. H_2/CO_2 selectivities and H_2 permeabilities of MOF membranes were computed as 2.1 × 10^{-5}−6.3 and 230−1.7 × 10^6 Barrer, respectively. A high number of MOF membranes was identified to surpass the upper bound defined for polymers due to high gas permeabilities of MOFs. Structure−performance relations revealed that MOFs with narrow pore sizes and low porosities are the best adsorbent materials for separation of CO_2 from H_2, whereas MOFs with large pore sizes and high porosities are the best membrane materials for selective separation of H_2. Our results will guide the selection of MOF adsorbents and membranes for efficient H_2 purification and CO_2 capture processes.



KEYWORDS: *metal organic frameworks, H_2 purification, CO_2 capture, pressure swing adsorption, membrane, molecular simulations*

Downloaded via KOC UNIV on April 9, 2019 at 08:06:06 (UTC).
See https://pubs.acs.org/sharingguidelines for options on how to legitimately share published articles.

1. INTRODUCTION

Carbon dioxide (CO_2) is a greenhouse gas, and its removal from industrial gas streams such as syngas, natural gas, and biomass gasification is essential. Syngas can be produced from coal-powered integrated gasification combined cycle systems effectively equipped with a precombustion CO_2 capture, where CO_2 is separated from H_2. Efficient CO_2 removal from syngas is a challenge since most of the adsorption process is done by amine scrubbing, an energy-intensive process.[1] Zeolites and activated carbons have been used as adsorbents to remove CO_2 from syngas, but their low CO_2 working capacities at syngas working conditions (20−40 °C, up to 40 bar)[2] hinder usage both in pressure swing adsorption (PSA) and in vacuum swing adsorption (VSA) processes. Alternatively, CO_2 can be captured using a membrane-based separation system. Polymeric membranes have been widely used for H_2/CO_2 separation, but they suffer from either low selectivity or low gas permeability in addition to the plasticization problem induced by CO_2 especially at high temperatures.[3,4] Zeolite membranes have high H_2/CO_2 selectivity and good thermal stabilities,[5] but they have limited structural tunability and pore functionalization.[6] Therefore, there is an ongoing research to identify new adsorbent and membrane materials that can accomplish CO_2/H_2 separation with high performance.

Metal organic frameworks (MOFs) are metal complexes bonded with organic ligands that can form various morphologies as porous materials.[7] MOFs have emerged as promising materials because of their tailorable pore sizes, high surface areas, tunable chemical functionalities, and good thermal and mechanical stabilities.[8] MOFs can also form highly stable complexes when more than one type of metal complex or ligand is used, which enriches different types of MOFs that can be synthesized. Several thousands of MOFs have been synthesized and tested for a wide range of applications including gas storage and separation,[9] drug storage and delivery,[10] and catalysis.[11] MOFs have been considered as promising materials for CO_2 capture due to their exceptional physicochemical properties, and several excellent review articles exist on CO_2 separation using MOFs as adsorbents and membranes.[12−15] Experimental studies on CO_2/H_2 separation generally measured single-component CO_2 and H_2 adsorption in MOFs and reported selectivities.[16,17]

MOFs can be highly promising materials in adsorption and membrane-based gas separation applications, but there is a need to define the best performing materials for each process.

Received: July 27, 2018
Accepted: September 7, 2018
Published: September 7, 2018

© 2018 American Chemical Society

DOI: 10.1021/acsami.8b12746
ACS Appl. Mater. Interfaces 2018, 10, 33693−33706

Due to the increasing number of MOF structures, experimental performance measurement for several thousands of MOF structures is not practical. High-throughput computational screening studies have a significant role in identification of the most promising materials among many for a desired application. Although several large-scale computational screening studies exist on the adsorption and membrane-based gas separation of CO_2/CH_4, CO_2/N_2, and CH_4/H_2 using MOFs,[18−21] studies on CO_2/H_2 separation are very limited in the literature. Qiao et al.[22] investigated adsorption and membrane selectivities of 8 amine-functionalized MOFs, identified from computationally screening, for CO_2/H_2 separation. They reported CO_2/H_2 adsorption selectivity of MOFs in the range of 2−72 at 1 bar and 298 K. Tong et al.[23] investigated 46 covalent organic frameworks (COFs) for separation of CO_2/H_2:20/80 mixture at 10 bar and 298 K. Two types of COFs exhibiting a CO_2/H_2 selectivity of 500−800 and CO_2 working capacity of 2.5−4 mol/kg were found to be comparable to or even better than traditional zeolites, NaY and AFX. Park et al.[24] computed single-component CO_2 adsorption capacities of 477 MOF structures existing in the CoREMOF (Computation-Ready, Experimental Metal Organic Frameworks) database at subambient conditions. They identified 20 MOFs with high CO_2 working capacities, >10 mol/kg. However, CO_2/H_2 selectivities of MOFs were not reported since only single-component CO_2 adsorption was studied. Chung et al.[25] used a genetic algorithm to screen hypothetical MOFs (hMOFs) in terms of CO_2 working capacity, CO_2/H_2 adsorption selectivity, and adsorbent performance score. Structural characteristics from the top 1% of 730 hMOFs defined by the genetic algorithm were used as a selection criterion to choose real MOFs from the CoREMOF database. Seventy-five and 99 MOFs were selected based on CO_2 working capacities and CO_2/H_2 adsorption selectivities, respectively. CO_2 working capacity and CO_2/H_2 selectivity of the best MOF was reported to be 7 mol/kg and 1000, respectively. Krishna and van Baten[26] examined membrane-based CO_2/H_2 separation performances of 6 different MOFs including widely studied ones such as IRMOF-1 and CuBTC and compared them with traditional zeolite membranes DDR, CHA, NaX, and NaY. They showed that MOF membranes have higher CO_2 permeabilities but lower CO_2/H_2 selectivities than zeolite membranes.

This literature review suggests there is a strong need for high-throughput computational screening of MOFs both for adsorption- and membrane-based CO_2/H_2 separations. In this work, we aimed to investigate both adsorbent and membrane performances of MOFs to efficiently separate CO_2 from syngas and enrich H_2 for the suitable industrial processes. For this aim, we focused on the most recent and complete MOF database[27] which has been carefully distinguished from non-MOF structures and maintained by the Cambridge Structural Database (CSD).[28] First, grand canonical Monte Carlo (GCMC) simulations were performed to calculate adsorption of CO_2/H_2:15/85 mixtures in MOFs at PSA and VSA conditions. Adsorption selectivity, working capacity, adsorbent performance score, and percent regenerability were computed for each MOF, and the top 20 promising MOFs were identified for each process. We also performed molecular simulations for $CO_2/H_2/CO/CH_4/H_2O$:15/75/5/5/0.1 mixtures to investigate the effect of a trace amount of water on the CO_2/H_2 selectivities of the best MOF adsorbents. We then performed molecular dynamics (MD) simulations and combined them with the GCMC results to evaluate membrane-based CO_2/H_2 separation performances of MOFs. Gas permeabilities and membrane selectivities of MOFs were calculated for CO_2/H_2 separation and compared with well-known zeolite and polymer membranes. The top 20 MOF membranes offering high H_2 selectivity and high H_2 permeability were identified. Similar calculations were also performed to identify the reverse selective membranes that offer high CO_2 selectivity from H_2 and high CO_2 permeability. Finally, the influence of structural properties of materials such as pore size, porosity, surface area, and metal type on the CO_2/H_2 separation performances of MOF adsorbents and membranes was elucidated to identify the characteristics of the best performing MOFs. This work is the first study in the literature that explores and compares adsorbent and membrane performances of MOFs for CO_2/H_2 separation. Our results will provide guidance to select the best MOF adsorbents and membranes for H_2 purification and CO_2 capture at specific operating conditions.

2. COMPUTATIONAL METHODS

2.1. MOF Database. We used the most comprehensive set of MOFs that was integrated with the CSD in the literature.[27] There were 54 808 structures cleaned from solvents using the Python code[27] available in the literature, and the structural properties of MOFs such as the pore limiting diameter (PLD), largest cavity diameter (LCD), accessible gravimetric surface area (SA), and porosity (ϕ) were calculated using Zeo++ software.[29] A simple Monte Carlo integration technique where the probe molecule is rolled over the MOF surface is used to calculate SA. A nitrogen-sized (3.7 Å) probe molecule was randomly inserted around each of the framework atoms and checked for overlap. The fraction of the probe molecules that did not overlap with other atoms was used to calculate SA. Walton and Snurr[30] showed that BET surface areas calculated from the simulated N_2 isotherms agree very well with the accessible surface areas calculated directly from the crystal structures in a geometric fashion. MOFs with zero accessible gravimetric SAs were eliminated, and structures with PLDs > 3.30 Å were selected so that both gas molecules (H_2 and CO_2 having kinetic diameters of 2.96 and 3.30 Å, respectively) can pass through adsorbents' and membranes' pores. A small number of MOFs (21) was eliminated since they did not reach conversion during the charge assignment process. After these refinements we ended up with 3857 diverse MOF structures representing a wide variety of structural and chemical properties. We used Zeo++ to identify MOFs that have open metal sites and concluded that 1686 out of 3857 MOFs have open metal sites.

2.2. Molecular Simulations. We used the same molecular simulation techniques that we applied in our previous studies to examine adsorption-based[31] and membrane-based[21] CH_4/H_2 separation with MOFs. All simulations were carried out using RASPA software.[32] We performed GCMC and MD simulations to calculate adsorption and diffusion properties of CO_2 and H_2 in MOFs, respectively. The potential parameters of MOFs were assigned from the Universal Force Field (UFF).[33] Usage of UFF for material screening purposes seems to be reasonably well justified by comparing molecular simulations with the experimental CO_2 and H_2 uptakes and diffusivities in several MOFs as demonstrated in previous works.[34,35] We showed the good agreement between simulated H_2 uptake and the experimentally reported data of a variety of MOFs including many subfamilies such as Bio-MOFs, COFs, CPOs, IRMOFs, PCNs, and ZIFs.[36] We also showed very good agreement between experimental and simulated H_2 adsorption isotherms of widely studied MOFs such as IRMOF-1, CuBTC, UiO-66, and ZIF-8 at various temperatures and in a large pressure range (77 K, 298 K, from 0.1 to 100 bar) in our recent work.[37] Similarly, we showed a good agreement between experimental and simulated CO_2 adsorption isotherms of many different well-known MOFs such as ZIFs, PCNs, and bio-MOFs (273

DOI: 10.1021/acsami.8b12746
ACS Appl. Mater. Interfaces 2018, 10, 33693−33706

K, 298 K from 0.1−10 bar) in our previous studies where we used the same simulation approach.[31,38−40]

Gas−gas and gas−MOF interactions were defined using Lennard−Jones (LJ) potential. The single-site spherical LJ 12-6 potential was used to model H_2.[41] A three-site rigid molecule with LJ 12-6 potential was used to model CO_2, and locations of the partial point charges were set as the center of each side.[42] In the molecular simulations of a 5-component mixture, $CO_2/H_2/CO/CH_4/H_2O$, CO was modeled using four-site model developed by Piper et al.,[43] CH_4 was modeled using a single-site spherical LJ 12-6 potential,[44] and H_2O was represented using the TIP4P model.[45] Lorentz−Berthelot mixing rules were employed for pair interactions. Electrostatic interactions were modeled using the Coulomb potential for CO_2 since it has quadrupolar moment. The charge equilibration (QEq) method implemented in RASPA was used to assign partial point charges to MOF atoms to compute electrostatic interactions between CO_2 molecules and MOFs, which were calculated by the Ewald summation.[46]

For gas adsorption at infinite dilution, Henry's constants (K^0) of CO_2 and H_2 molecules were calculated at the zero-coverage using 10^5 moves by the Widom particle insertion method. The isosteric heat of adsorption of gas molecules (Q_{st}^0) was also computed at infinite dilution from these simulations. GCMC simulations for CO_2/H_2:15/85 mixtures were performed at 298 K and three different pressures, 0.1, 1, and 10 bar. In mixture GCMC simulations, four different types of moves were considered for H_2 including translation, reinsertion, swap of a molecule, and identity exchange. For CO_2, an additional move, rotation, was defined to account for rotational degree of freedom. The Peng−Robinson equation of state was used to change the pressure to the fugacity. The intermolecular interactions were truncated at the cutoff distance of 13 Å. Simulation cell lengths were expanded to at least 26 Å along each dimension, and periodic boundary conditions were applied in all dimensions. GCMC simulations were carried out for each MOF using 10 000 cycles where the first 5000 cycles were for initialization and the last 5000 cycles were for taking ensemble averages.

In order to calculate single-component self-diffusivities (D^0) of CO_2 and H_2, we performed MD simulations. We switched off gas−gas intermolecular interactions and inserted 30 gas molecules into each MOF to represent the infinite dilution condition in order to obtain high accuracy. MD simulations were performed for 10^6 cycles in the NVT ensemble using a time step of 1 fs. We used 1000 initialization cycles and 10 000 equilibration cycles. The Nose−Hoover thermostat[47] was used in NVT-MD simulations. From the slope of the mean square displacement of gas molecules, we calculated the self-diffusion coefficients of gases. Finally, we performed mixture MD simulations by using appropriate gas loadings determined from the GCMC simulations performed at 1 bar and 298 K. We included both gas−gas and gas−-framework interactions for diffusion simulations of gas mixtures. At least three trajectories were used to compute self-diffusivities of each component. In order to save computational time in molecular simulations, MOFs were assumed to be rigid. Framework flexibility has considerable effects on MOFs which have narrow pores having similar sizes with those of target gas molecules.[48] The MOFs we considered have pore sizes greater than the kinetic diameter of both gas molecules; therefore, flexibility is assumed to have a negligible effect on our results.

2.3. Calculations for Adsorbents and Membranes. CO_2 can be effectively separated from H_2 through PSA and VSA processes.[49] Therefore, we investigated adsorption-based separation performances of MOFs both for PSA and for VSA processes. The composition of the gas mixture, adsorption and desorption pressures, and temperature were set to represent the industrial precombustion CO_2 capture process following the literature.[50] In order to mimic the PSA (VSA) process, adsorption and desorption pressures were set to 10 (1) and 1 (0.1) bar, respectively, at 298 K in the simulations. Table 1 provides adsorption and membrane selection metrics considered in this study. Selectivity is considered as the most important metric in choosing adsorbents. Adsorption selectivity is the ratio of the strongly adsorbed gas (CO_2) to the weakly adsorbed one (H_2). A high working capacity

Table 1. Metrics Used To Evaluate MOF Adsorbents and Membranes[a]

metrics	formula
adsorption selectivity	$S^0_{ads,CO_2/H_2} = \frac{K^0_{CO_2}}{K^0_{H_2}}$
mixture adsorption selectivity	$S^{mix}_{ads,CO_2/H_2} = \frac{N_{CO_2}}{N_{H_2}} \Big/ \frac{y_{CO_2}}{y_{H_2}}$
working capacity	$\Delta N_i = N_{ads,i} - N_{des,i}$
adsorbent performance score	$APS = S^{mix}_{ads,CO_2/H_2} \times \Delta N_{CO_2}$
percent regenerability	$R\% = \frac{\Delta N_{CO_2}}{N_{ads,CO_2}} \times 100\%$
diffusion selectivity	$S^0_{diff,H_2/CO_2} = \frac{D^0_{H_2}}{D^0_{CO_2}}$
mixture diffusion selectivity	$S^{mix}_{diff,H_2/CO_2} = \frac{D^{mix}_{H_2}}{D^{mix}_{CO_2}}$
membrane selectivity	$S^0_{mem,H_2/CO_2} = S^0_{ads,H_2/CO_2} \times S^0_{diff,H_2/CO_2}$
mixture membrane selectivity	$S^{mix}_{mem,H_2/CO_2} = S^{mix}_{ads,H_2/CO_2} \times S^{mix}_{diff,H_2/CO_2}$
permeability at infinite dilution	$P^0_i = K^0_i \times D^0_i$
mixture permeability	$P^{mix}_i = \frac{N^{mix}_i \times D^{mix}_i}{f_i}$

[a] N_{ads}: gas uptake in the mixture at 10 bar for PSA and 1 bar for VSA. N_{des}: gas uptake in the mixture at 1 bar for PSA and 0.1 bar for VSA. i: gas species, CO_2 or H_2. K^0: Henry's constant at infinite dilution. D^0: self-diffusivity at infinite dilution. D^{mix}: self-diffusivity of gas species in the mixture. y: composition of the gas species in the bulk phase. f: partial pressure of gas species in the mixture. 1 Barrer = 3.348×10^{-16} mol × m/(m² × s × Pa).

is desired for lower energy cost through less frequent regeneration cycles and a smaller system volume.[51] Working capacity is the difference between the CO_2 uptakes at the adsorption and desorption pressures, corresponding to 10 and 1 bar for PSA and 1 and 0.1 bar for VSA, respectively. We used the feed-gas composition for both the adsorption and the desorption conditions following the literature.[23,26,52] Snurr's group[25] recently visited the definition of working capacity and showed that the gas-phase composition along the column is identical to the composition of the mixture fed to the column at the adsorption. However, the gas phase was found to be almost pure CO_2 throughout the column at the end of the depressurization step. Therefore, they proposed that CO_2 uptake at desorption should be calculated assuming a pure CO_2 gas in defining the working capacity. In this work, we used the conventional definition of CO_2 working capacity and set the composition of gas phase in desorption conditions as the same composition in the feed. Therefore, our computed working capacities may be overestimating the practical ones. Adsorbent performance score (APS) accounts both for the adsorption selectivity and for the working capacity as shown in Table 1. Another important metric is the percent regenerability (R%), which is generally desired to be >85% in order to increase the amount of product per cycle. It is calculated as the ratio of working capacity over gas uptake calculated at 10 and 1 bar for PSA and VSA, respectively. In this work, we calculated all adsorbent selection metrics from molecular simulations of binary CO_2/H_2 mixtures. We compared adsorption selectivities of MOFs computed at infinite dilution with the selectivities computed for binary CO_2/H_2:15/85 mixtures at 0.1, 1, and 10 bar in Figure S1. Selectivities calculated using single-component data at infinite dilution correlated well with the mixture selectivities at low pressures, but they gradually deviated as the pressure increases. Mixture adsorption selectivities were found to be lower than the infinite dilution selectivities at higher loadings due to the competition between CO_2 and H_2 molecules for the same adsorption sites in the MOFs' pores. Therefore, we used binary CO_2/H_2 mixture simulations rather than infinite dilution condition both for the PSA and for the VSA processes. There are two significant metrics generally used to select the membrane materials, permeability and

DOI: 10.1021/acsami.8b12746
ACS Appl. Mater. Interfaces 2018, 10, 33693−33706

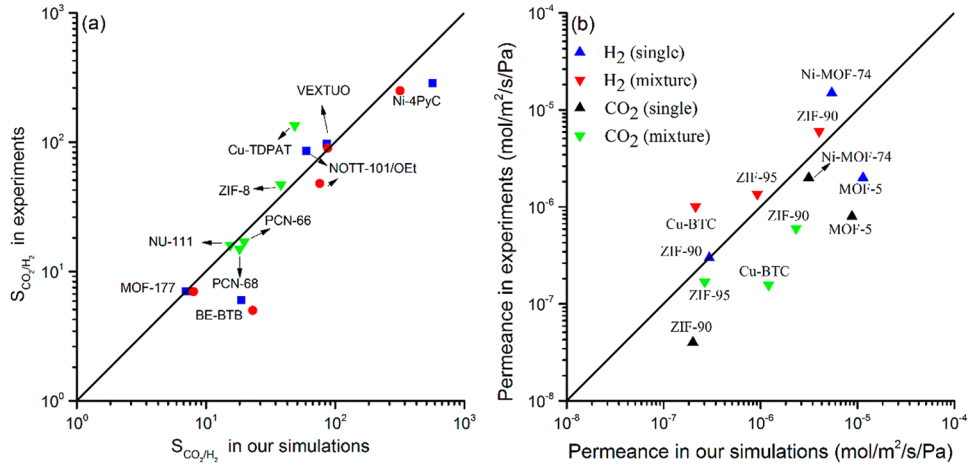


Figure 1. Comparison of experimental and simulated (a) adsorption selectivities of various MOFs and (b) gas permeances of MOF membranes. Details of the experimental data are given in Tables S1 and S2. Colors in a correspond to different adsorption pressures as listed in Table S1.

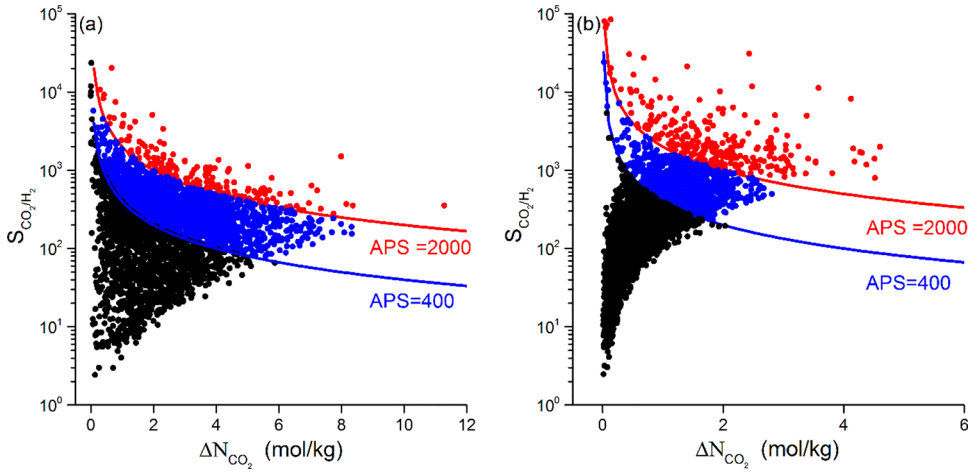


Figure 2. Relation between adsorption selectivity, working capacity, and APS of MOFs for CO_2/H_2:15/85 mixture at (a) PSA and (b) VSA conditions. Black, blue, and red points represent MOFs with APS < 400, 400 < APS < 2000, APS > 2000, respectively.

selectivity. Gas permeability of a membrane is generally driven by the mutual effect of adsorption and diffusion and calculated by the product of them as shown in Table 1. While high gas permeability is needed for low investment and operation cost, high selectivity is required to obtain high-purity products. Membrane selectivity is described as a measure of the efficiency of a membrane to separate one gas from another. It is calculated by the ratio of permeability of the more permeable gas to the less permeable one as shown in Table 1.

We first compared the results of our molecular simulations with the available experimental data of MOF adsorbents and membranes to confirm the accuracy of our computational approach. Figure 1a compares experimentally measured CO_2/H_2 adsorption selectivities of various MOFs taken from the literature with the selectivities computed in this work under identical conditions. Our simulation results agree well with the experiments over a wide range of conditions as listed in Table S1 together with the corresponding references. We also included selectivities from previous simulation studies, which are also in a good agreement with the selectivities computed in this work, validating the applicability of molecular simulations for assessing MOF adsorbents' selectivities. We also showed the good agreement between experimentally measured and simulated CO_2 and H_2 isotherms of these MOFs in Figure S2. Several experimental studies measured CO_2 and H_2 permeances, permeability divided by the membrane thickness, through MOF membranes. Figure 1b shows the good agreement between experimentally measured CO_2 and H_2 permeances (both single-component and mixture) of MOF membranes such as Ni-MOF-74, MOF-5 (IRMOF-1), CuBTC, ZIF-90, and ZIF-95 with the permeance predictions of our molecular simulations carried out at the same conditions. Experimental conditions such as feed and permeate pressures, membrane thickness, and related references are listed in Table S2. Motivated from these good agreements, we carried out our high-throughput simulations for 3857 MOFs and examined their adsorption-based and membrane-based CO_2/H_2 separation performances. Throughout this manuscript we represented the gas mixture either as CO_2/H_2 or as H_2/CO_2 where the first component represents the selected one over the second component. In other words, the section on adsorption-based gas separation discusses CO_2 separation from H_2 (CO_2/H_2), whereas in the membrane-based gas separation section, we considered both CO_2-selective (CO_2/H_2) and H_2-selective (H_2/CO_2) membranes.

3. RESULTS AND DISCUSSION

3.1. MOF Adsorbents. Figure 2 shows the CO_2/H_2 selectivity and CO_2 working capacity of MOFs at PSA and VSA conditions. CO_2/H_2 selectivities of MOFs at PSA (VSA) are in the range of 2.43−24490 (2.47−84356), and CO_2 working capacities at PSA (VSA) are between 0.001 and 11.28 (0.007 and 4.60) mol/kg. MOFs offering high CO_2/H_2 selectivities (>5000) mostly have low CO_2 working capacities

DOI: 10.1021/acsami.8b12746
ACS Appl. Mater. Interfaces 2018, 10, 33693−33706

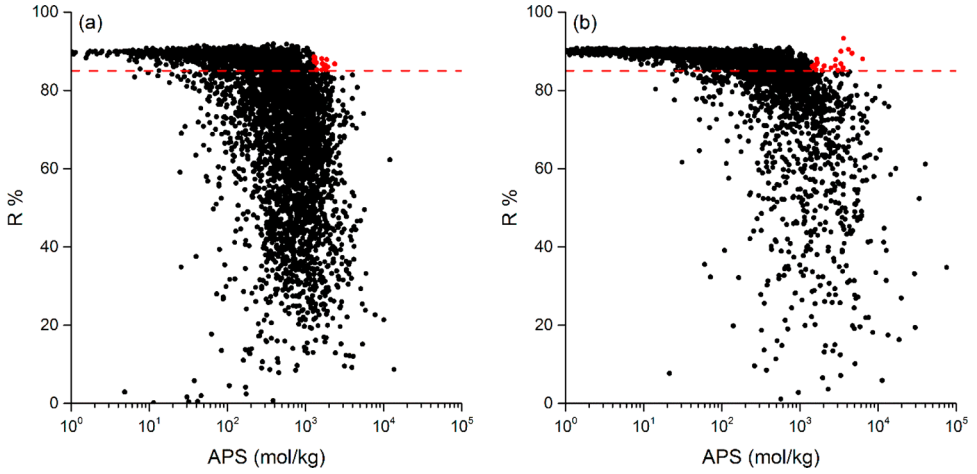


Figure 3. *R*% and APS of MOFs computed for CO_2/H_2:15/85 mixture for (a) PSA and (b) VSA conditions. Red dotted line shows the minimum desired *R*% = 85%. Red data points represent the top MOF adsorbents with the highest APSs and *R*% > 85%.

(<2 mol/kg) both in PSA and in VSA processes. Similarly, there are many MOFs having high CO_2 working capacities, but they have low selectivities, preventing them from becoming promising candidates. On the other hand, MOFs with high CO_2 working capacities (~8 mol/kg for PSA and ~4 mol/kg for VSA) exhibit moderate CO_2/H_2 selectivities, ~200 for PSA and ~2000 for VSA. An ideal adsorbent efficiently adsorbs/desorbs the target gas without compromise between selectivity and capacity. Therefore, we computed APS and defined two arbitrary limits shown by the red and blue curves in Figure 2 to identify the promising materials. Blue points represent the MOFs which offer a good combination of selectivity and working capacity resulting in APS > 400, whereas red points show the most promising MOF adsorbents having the best combination of selectivity and working capacity resulting in APS > 2000. One hundred seventy six (276) out of 3857 MOFs were located above the red line for the PSA (VSA) process. CO_2/H_2 selectivity of these most promising MOFs was computed as 280−20 357 (798−84 350), and CO_2 working capacities were computed as 0.29−11.28 (0.028−4.60) mol/kg in PSA (VSA) as shown in Figure 2a (Figure 2b).

It is a good practice to compare MOFs with traditional adsorbents, zeolites. Fang et al.[53] examined the CO_2 working capacity of cationic zeolites for PSA and VSA processes regardless of the second gas component. The highest CO_2 working capacities of the 10-membered ring (10MR) zeolites were reported as 1.95 and 2.03 mol/kg for PSA and VSA processes, respectively. Higher capacities, 7.48 and 6.18 mol/kg, were reported for zeolites having large pore volumes for PSA and VSA, respectively. If we compare MOFs with zeolites, 2137 and 166 MOFs outperform 10MR zeolites at PSA and VSA conditions. Eleven MOFs exceed the performance of cationic zeolites with large pore volumes at PSA conditions, whereas there is no MOF that can outperform zeolites having large pore volumes at VSA conditions. Krishna[54] performed molecular simulations for many zeolites including NaY, CHA, FAU, and LTA and reported that NaX and NaY are the most CO_2/H_2-selective materials with selectivities of 1510 and 550, respectively at 10 bar and 300 K for a CO_2/H_2:15/85 mixture. NaX and NaY zeolites have lower selectivities and lower APSs (~29.6 and ~27.1 mol/kg) compared to MOFs under PSA conditions. Both experimental studies for CO_2 uptakes of NaX (4.5 mol/kg) and NaY (3.9 mol/kg)[55−57] and simulations (~5.3 for NaX and ~4.8 mol/kg for NaY)[54] showed that these zeolites also have lower CO_2 uptakes than MOFs. Chung et al.[25] evaluated CO_2 working capacity, CO_2/H_2 adsorption selectivity, and APS for 730 hypothetical MOFs (hMOFs). Comparison between hMOFs and real, synthesized MOFs we examined in this work reveals that although hMOFs can reach the performance of real MOFs in terms of CO_2 working capacity, they have much lower selectivities and APSs than the real MOFs. We identified 193 MOFs with CO_2/H_2 adsorption selectivities > 1000 at 10 bar, but there were only 6 hMOFs with selectivities > 1000 and among them the highest selectivity was 2600. We found that 176 MOFs have APS > 2000 mol/kg, as illustrated in Figure 2a, whereas no hMOF was reported to have APS > 1200 mol/kg. Overall, all these comparisons showed that MOFs are either comparable to or even better than the zeolites in adsorption-based CO_2/H_2 separations, and they perform much better than hMOFs. It is important to note that even if hMOFs were shown to have better separation performances, some of these structures may not be readily synthesizable.

The relation between *R*% and APSs of MOFs in PSA and VSA applications is shown in Figure 3a and 3b, respectively. MOFs having high APSs generally suffer from low *R*%. *R*% values of MOFs vary from 0.16% (1.14%) to 91.88% (93.30%) in PSA (VSA) processes. The number of MOFs exhibiting *R*% > 85% is 1060 (2625) at PSA (VSA) conditions. We identified the top 20 MOFs with the highest APSs and *R*% > 85% for both processes as shown with red points in Figure 3. Table 2 lists APS, *R*%, and adsorption selectivity of the top 20 MOFs for PSA and VSA processes together with the structural properties of these materials. Results suggest that promising MOFs for a VSA process tend to have higher selectivities ranging from 550 to 2400, whereas this range is between 155 and 485 for the PSA process. DABWUA was identified as the best adsorbent for a PSA process with a CO_2/H_2 selectivity of 322 and *R*% of 87% at 10 bar and 298 K. High gas adsorption performance of DABWUA was attributed to its narrow pore geometry in the literature,[58] which increases the accessibility of the adsorption sites available on the surface of framework. DATKIU was identified as the best adsorbent for a VSA process with a selectivity of 1405 and *R*% of 88% at 1 bar and 298 K in Table 2. This can be attributed to the existence of the

DOI: 10.1021/acsami.8b12746
ACS Appl. Mater. Interfaces 2018, 10, 33693−33706

Table 2. Separation Performances of the top 20 MOFs (having the highest APSs and $R\%$ > 85%) for PSA and VSA Processes

MOFs	APS (mol/kg)	$S^{mix}_{ads,\ CO_2/H_2}$	$R\%$	LCD (Å)	PLD (Å)	ϕ	SA (m^2/g)
pressure swing adsorption (PSA)							
DABWUA	2364.66	322.31	86.76	6.33	3.84	0.64	1367.86
HOWRES	1931.12	299.70	85.98	5.94	5.11	0.63	1511.89
ENATUJ	1872.19	241.81	87.88	5.92	5.35	0.69	2625.32
HUFHUN	1818.42	484.51	85.32	10.40	8.17	0.54	742.06
IJEFUZ	1797.25	287.58	86.42	6.27	5.40	0.65	2095.14
CECJAW	1737.22	292.02	86.12	5.62	4.51	0.65	2173.37
VARJEF	1715.09	233.07	86.43	7.50	4.27	0.63	2105.15
TUBTOB	1646.22	206.05	86.83	5.78	4.11	0.65	2672.89
AQEKUD	1614.35	221.62	88.07	4.87	4.21	0.70	2724.6
NULHEJ	1608.33	356.56	85.19	7.18	5.90	0.54	874.847
HASSUR	1393.04	250.94	85.24	7.03	5.33	0.63	1847.89
FOJWOS	1370.69	193.03	87.04	8.40	5.00	0.65	2302.56
LONVIV	1323.25	235.23	88.41	10.8	9.68	0.62	1042.60
UWOWEJ	1310.74	188.27	87.93	6.45	5.23	0.67	2998.37
XUNGIX	1299.81	177.96	88.31	8.23	4.89	0.66	3065.15
QUQQUP	1299.14	160.68	88.61	5.16	4.78	0.69	4342.4
CAXTEC	1298.04	215.68	87.73	10.87	5.27	0.63	1874.49
LEYGIH	1293.71	219.00	87.29	5.67	4.14	0.64	2102.15
HAFVUH	1293.23	219.80	88.60	7.25	7.14	0.60	1539.15
COQTEJ	1288.85	154.71	87.49	7.76	6.26	0.70	3263.67
vacuum swing adsorption (VSA)							
DATKIU	6339.10	1404.82	88.05	5.74	4.50	0.64	2149.07
NIDBOS	4635.11	2060.24	89.50	5.46	5.27	0.48	539.12
HISJIE	4196.19	2401.78	90.47	6.28	5.58	0.43	361.15
EGELUY	3605.94	798.31	93.30	7.19	6.77	0.63	1554.21
AFEJOK	3569.22	1154.36	85.78	5.98	5.12	0.58	1257.63
GUKYUI	3353.50	1654.38	89.97	5.99	5.23	0.49	543.66
RAVNAE	3337.80	1650.24	86.83	4.58	4.25	0.53	376.57
PEJMOH	3055.10	1111.24	85.17	4.78	4.06	0.53	842.18
YAZFOW	2843.27	896.47	87.87	7.44	7.30	0.61	1108.06
RIGVOU	2834.71	2096.43	86.32	5.38	5.16	0.40	296.13
WOBQEL	2487.58	824.07	85.76	6.08	5.37	0.55	1053.12
UBIPAY	2044.71	923.13	86.27	4.39	3.96	0.49	651.70
BUHJUL	1922.78	790.80	85.18	5.38	4.57	0.51	880.20
OTAQUW	1670.33	969.23	87.02	5.80	4.62	0.52	886.78
CUSDIE	1646.45	629.68	88.00	13.09	5.58	0.67	1576.51
AMOYOR	1622.25	1003.13	86.63	4.84	4.51	0.47	470.55
YEVPIZ	1617.61	747.94	85.25	4.51	3.84	0.55	741.98
YARFII02	1526.45	756.33	86.45	5.48	4.20	0.52	809.62
EBIDAW	1456.33	693.99	85.94	5.45	4.04	0.54	830.57
TIXVON	1441.87	557.29	86.18	5.07	3.92	0.58	1034.39

extra framework ions, BF_4^- in the framework, which enhances CO_2 adsorption. In order to confirm this, we repeated adsorption simulations by switching off the CO_2−MOF electrostatic interactions. CO_2 adsorption at 0.1 (1) bar severely dropped from 0.612 (5.12) to 0.026 (0.25) mol/kg when the electrostatic interactions were neglected. Similarly, CO_2/H_2 adsorption selectivity computed at 0.1 (1) bar decreased from 1405 (322) to 40 (171), confirming the strong electrostatic interactions between CO_2 and MOF. In addition, DATKIU and 13 MOFs out of the top 20 materials identified for VSA application were found to have 1-D channels. Previous studies on MOFs with 1-D channels showed that this type of material generally exhibits good gas separation performance since gas molecules contact more with the framework due to continuous pore length in 1-D channels.[20,26] At that point, we would like to note that making sure that the final structure is correct after the initial screening approach is very important because the conclusion about the MOF's performance strongly depends on the correctness of the final structure. Therefore, we carefully examined the structures of the top adsorbent materials to make sure that these MOFs do not have any problems such as missing extra framework cations or remaining solvent molecules.

One interesting feature of Table 2 is that there is no common promising MOF for PSA and VSA processes since adsorption performances of MOFs change when the operating pressure is altered. In order to understand how well the MOF rankings in PSA and VSA conditions correlate with each other, we computed Spearman's ranking correlation coefficient (SRCC), which is used as a measure of the relationship between two independent ranking lists. SRCC varies between −1 and 1 and becomes unity if the correlation perfectly matches in two independent rankings. Table 3 shows the SRCC values computed for the ranking of all 3857 MOFs for

DOI: 10.1021/acsami.8b12746
ACS Appl. Mater. Interfaces 2018, 10, 33693−33706

Table 3. SRCC Values for the MOF Rankings of PSA and VSA Processes

metrics used to rank MOFs	SRCC	no. of common MOFs in top 20 lists
$S^{mix}_{ads,H_2/CO_2}$ (0.1 bar)	0.81	4
$S^{mix}_{ads,H_2/CO_2}$ (1 bar)	0.83	4
$S^{mix}_{ads,H_2/CO_2}$ (10 bar)	0.84	6
APS (mol/kg)	0.97	13
R%	0.50	1
ΔN_{CO_2} (mol/kg)	0.93	19
ΔN_{H_2} (mol/kg)	0.97	9

PSA and VSA processes in terms of selectivity, working capacity, APS, and *R*%. Table 3 presents that SRCC values between PSA and VSA rankings are higher than 0.8 for all metrics except *R*%, indicating that there is a high correlation between ranking of MOFs for PSA and VSA in terms of selectivity, working capacity, and APS. That means a MOF showing high selectivity/working capacity in the PSA process is very likely to have high performance in the VSA process, but the same is not valid for *R*%. Table 3 also shows the number of common promising MOFs in the top 20 MOF lists of PSA and VSA processes. There were 19 common MOFs in CO_2 working capacity lists of PSA and VSA, while there is only one MOF that is common in *R*% lists. These results strengthen the observations from Table 2 and imply that MOFs should be chosen to achieve PSA and VSA processes with high efficiency considering the combination of these three performance metrics.

It is worth mentioning that the MOFs we investigated have already been synthesized, but the adsorbent performances of most of them have not been proven yet. A detailed search for the top 20 MOFs was done to see if any experimental study reported their CO_2 and H_2 adsorption performances. Lässig et al.[58] reported CO_2 and H_2 uptakes of DABWUA, the top material of the PSA process, as 9.2 and 15.2 mol/kg at 273 and 77 K, respectively, at 1 bar. We carried out GCMC simulations at the same conditions and obtained a very good match with the experimental data, 9.7 and 17.4 mol/kg of CO_2 and H_2 uptakes, respectively. Experimental gas adsorption data was also available for one of the top MOFs of the VSA process, YAZFOW.[59] While the CO_2 uptake of YAZFOW was experimentally reported as 6.3 mol/kg at 1 bar and 273 K, we calculated its CO_2 adsorption as 7.5 mol/kg using GCMC simulations under the same pressure and temperature. These comparisons show that our molecular simulations make accurate estimates for the adsorption-based separation performances of MOFs.

In precombustion conditions, a trace amount of water is present. Previous studies showed that due to the strong interactions between highly polar water molecules and MOFs, a trace amount of water in the gas phase can significantly alter adsorption selectivities of MOFs.[60−62] The challenge of maximizing the CO_2 adsorption capacity while minimizing the H_2O adsorption capacity of MOFs for the gas mixtures including water vapor was discussed for porous adsorbents.[63] Li et al.[64] showed that the presence of water vapor even in small mole fractions (0.1) decreases the CO_2/H_2 adsorption selectivity of rht-MOF since H_2O molecules compete with CO_2 for the available adsorption sites. In order to discuss the effect of water on the CO_2/H_2 separation performances of MOFs, we performed GCMC simulations for the top promising MOF of the PSA process, DABWUA, considering $CO_2/H_2/CO/CH_4/H_2O$:15/75/5/5/0.1 mixture at 10 bar. The CO_2 uptake and CO_2/H_2 selectivity were computed as 6.28 mol/kg and 200, respectively. These values were lower than the uptake and selectivity computed for binary CO_2/H_2:15/85 mixture, 8.45 mol/kg and 322, respectively. We also performed the same five-component gas mixture simulations for the top promising MOF of the VSA process, DATKIU, at 1 bar. The CO_2 uptake was computed to be 0.48 mol/kg, dramatically lower than that computed for the binary mixture, 5.12 mol/kg. Similarly, CO_2/H_2 selectivity was computed to be a lot lower, 293, than the one computed for the binary mixture, 1404. The high selectivity of DATKIU was explained by the presence of extra framework ions in the framework as we discussed above. Since highly polar water molecules occupy these adsorption sites, CO_2 adsorption is hindered and CO_2/H_2 selectivity decreases. Consequently, we conclude that presence of water vapor in the precombustion gas mixture has a more pronounced effecton the CO_2/H_2 selectivity of MOFs that have strong electrostatic interactions with CO_2 due to the presence of extra framework cations.

3.2. MOF Membranes. Separating H_2 from CO_2 is more advantageous in membrane applications due to the higher molar fractions in the stream and smaller kinetic diameter of H_2 than CO_2 which lets H_2 penetrate faster through the smaller pores of membranes. Therefore, we focused on selective separation of H_2 from CO_2 using MOF membranes in contrast to the selective separation of CO_2 from H_2 as we discussed above for MOF adsorbents. We first compared adsorption, diffusion, and membrane selectivity of MOFs calculated at infinite dilution for H_2/CO_2 separation in Figure 4. Adsorption favors CO_2 in all MOFs due to the strong

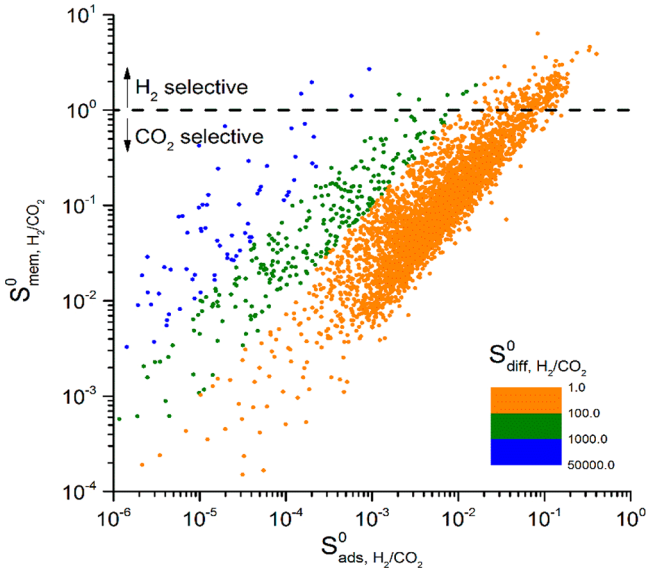


Figure 4. Comparison for adsorption, diffusion, and membrane selectivities computed at infinite dilution and 298 K.

interactions of CO_2 with the MOF atoms. Therefore, H_2/CO_2 adsorption selectivities of all MOFs are less than 1. Diffusion favors H_2 since lighter and weakly adsorbed H_2 molecules diffuse faster than CO_2. Therefore, diffusion selectivities of all MOFs are higher than 1, and we color coded them in Figure 4. Orange points represent the MOFs with low diffusion selectivities for H_2, whereas green points show the MOFs

DOI: 10.1021/acsami.8b12746
ACS Appl. Mater. Interfaces 2018, 10, 33693−33706

with mediocre/high diffusion selectivities. MOFs shown by blue have very high H_2/CO_2 diffusion selectivities, >1000. H_2 diffuses at least 3 orders of magnitude faster than CO_2 in these MOFs. When the diffusion selectivity favoring H_2 dominates the adsorption selectivity favoring CO_2, MOFs become H_2-selective membranes. Two hundred nine out of 3857 MOFs were identified to be H_2-selective membranes. MOFs having high adsorption selectivity for CO_2 ($S^0_{ads,H_2/CO_2} < 10^{-3}$) and very high diffusion selectivity for H_2 ($S^0_{diff,H_2/CO_2} > 1000$) as shown by blue points above the dotted line are H_2-selective membranes. MOFs having limited/low adsorption selectivity for CO_2 ($10^{-2} < S^0_{ads,H_2/CO_2} < 10^{-1}$) and low diffusion selectivity for H_2 ($1 < S^0_{diff,H_2/CO_2} < 100$) also become H_2-selective membranes as shown by orange points above the dotted line in Figure 4.

Figure 5 shows the trade-off between H_2 permeability and H_2/CO_2 selectivity of MOF membranes together with the well-known Robeson's upper bound[65] established for polymeric membranes. We used permeability rather than permeance in Figure 5 since the upper bound of polymeric membranes was defined based on permeability. $S^0_{mem,H_2/CO_2}$ values were computed to be between 2.10×10^{-5} and 6.34, whereas $P^0_{H_2}$ values were calculated in the range of 229.33−1.67 $\times 10^6$ Barrer. A significant number of MOFs (899) exceeds the upper bound, which suggests that MOF membranes can replace traditional polymeric membranes in selective separation of H_2 from CO_2. A remarkable number of MOFs (1716) exhibit very high H_2 permeability, $P^0_{H_2} > 10^5$ Barrer, as shown by blue points in Figure 5. We ranked the MOF membranes having $P^0_{H_2} > 10^5$ Barrer based on their H_2/CO_2 selectivity from the highest to the lowest and identified the top 20 MOFs based on this ranking. The top 20 most promising MOF membranes offering H_2/CO_2 selectivity > 2.27 and $P^0_{H_2} > 10^5$ Barrer are shown with red points in Figure 5. Gas separation performances of these top MOF membranes together with their structural properties are listed in Table 4. Adsorption selectivities of the top MOF membranes for CO_2 are generally lower than 10, whereas diffusion selectivities of MOFs for H_2 are generally larger than 12. As discussed above, top membranes are the MOFs where diffusion selectivity for H_2 dominates the adsorption selectivity for CO_2. Another interesting feature of Table 4 is that top MOFs are highly porous, $\phi > 0.8$, with large pore openings, LCDs > 10 Å. We will discuss these structure−performance relations in detail in the next section. Finally, we would like to note that we only considered the MOFs with pore sizes larger than 3.30 Å to let both gas molecules diffuse through the pores. Two ZIF (zeolitic imidazolate framework) membranes acting as molecular sieves for H_2/CO_2 separation were reported to be promising in the literature, but they were absent in our MOF database due to their narrow pore sizes (<3.30 Å). H_2/CO_2 selectivities of these membranes were measured to be high, 8.4−13.6 for ZIF-7[66,67] and 4.6−7.3 for ZIF-8,[68,69] but their H_2 permeabilities were quite low, 6.7×10^2−3.4×10^3 Barrer for ZIF-7 and 2.8×10^3−2.2×10^4 Barrer for ZIF-8, compared to the MOFs we examined in this study.

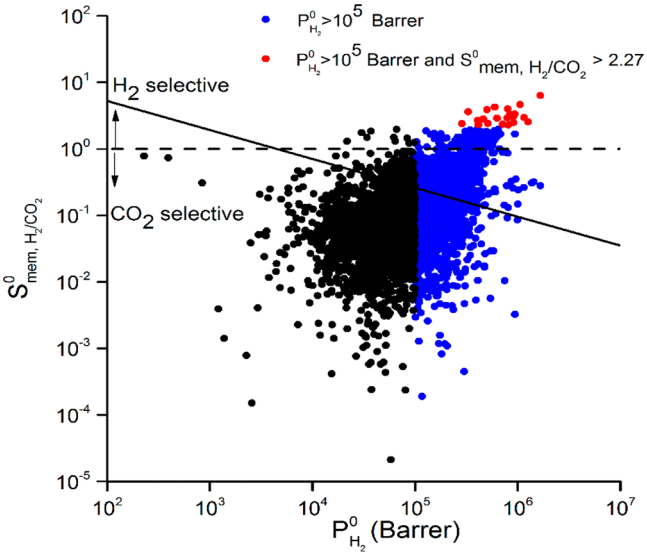


Figure 5. H_2/CO_2 selectivity and H_2 permeability of MOF membranes. Black dashed line indicates $S^0_{mem,H_2/CO_2} = 1$. Black solid line represents the upper bound for H_2/CO_2 separation.

Performing H_2/CO_2 mixture MD simulations is computationally demanding because the number of adsorbed H_2 molecules is very small compared to the large number of adsorbed CO_2 molecules and the simulation cells should be significantly extended to consider enough H_2 molecules for increasing the statistical accuracy of molecular simulations. Therefore, we performed the mixture MD simulations only for the top 20 MOF membranes. The composition of the CO_2/H_2 mixture was set to 15/85; the feed pressure was set to 1 bar at room temperature. Figure 6 shows that H_2 and CO_2 permeabilities computed at infinite dilution (P^0) agree well with the permeabilities computed for the binary mixture (P^{mix}). CO_2 (H_2) permeabilities in the mixture case are generally higher (lower) than those in the infinite dilution case due to the strong CO_2 adsorption preference of MOFs. Due to the competition between H_2 and CO_2, strongly adsorbed CO_2 hinders the adsorption of H_2 in the mixture and blocks the diffusion of H_2, leading to a reduction in H_2 permeability. As a result, H_2/CO_2 membrane selectivities of MOFs, which were calculated as the ratio of gas permeabilities, were found to be generally similar to or lower in the mixture case compared to the infinite dilution case as shown in the inset figure. These results suggest that infinite dilution simulations can be performed to obtain quick and reasonably accurate estimates for selectivities and gas permeabilities of MOF membranes. Finally, we searched for the experimental gas permeability data of the MOFs identified as the top H_2-selective membranes. None of these MOFs has been used to make membranes; therefore, it was not possible to make a comparison between experiments and simulations. Among the top MOF membranes we identified, FOTNIN,[70] RUTNOK,[71] and TOVKOG[72] have common names of PCN-777, IRMOF-77, and PCN-285, respectively, in the literature. These MOFs were reported to be highly stable, encouraging further research on fabrication of membranes using these materials.

Reverse selective membranes, which separate CO_2 from H_2, have also recently received interest for H_2 purification from synthesis gas. In these membranes the retentate stream is the main purified stream instead of the permeate. A few studies suggested MOFs as CO_2-selective membranes for CO_2/H_2 separation.[73,74] Therefore, we examined CO_2 permeability and CO_2/H_2 selectivity of MOF membranes together with the upper bound established for polymeric membranes[75] in Figure

DOI: 10.1021/acsami.8b12746
ACS Appl. Mater. Interfaces 2018, 10, 33693−33706

Table 4. Separation Performances of the top 20 MOFs for Membrane-Based Gas Separation[a]

MOFs	LCD (Å)	PLD (Å)	ϕ	$D^0_{CO_2}$ (cm^2/s)	$D^0_{H_2}$ (cm^2/s)	$P^0_{CO_2}$ (Barrer)	$P^0_{H_2}$ (Barrer)	$S^0_{ads,CO_2/H_2}$	$S^0_{diff,H_2/CO_2}$	$S^0_{mem,H_2/CO_2}$
FOTNIN	33.63	28.54	0.91	1.78×10^{-4}	1.35×10^{-2}	2.63×10^{5}	1.67×10^{6}	12.00	76.05	6.34
XANLIJ	26.20	14.45	0.91	6.19×10^{-4}	8.44×10^{-3}	2.30×10^{5}	1.06×10^{6}	2.95	13.62	4.61
JULDAV	7.54	6.53	0.88	4.50×10^{-4}	5.74×10^{-3}	1.42×10^{5}	5.98×10^{5}	3.02	12.78	4.23
TURFIX	26.88	14.28	0.90	3.74×10^{-4}	6.24×10^{-3}	2.01×10^{5}	8.04×10^{5}	4.18	16.69	3.99
XIJNUA	16.10	15.60	0.82	5.38×10^{-4}	5.15×10^{-3}	1.30×10^{5}	5.03×10^{5}	2.47	9.58	3.88
WIDNEC	13.84	12.53	0.76	1.00×10^{-4}	3.46×10^{-3}	9.20×10^{4}	3.30×10^{5}	9.65	34.65	3.59
ECOKAJ	18.97	17.57	0.88	4.59×10^{-4}	7.25×10^{-3}	2.82×10^{5}	9.34×10^{5}	4.77	15.81	3.31
RUBYUK	16.11	12.67	0.87	2.77×10^{-4}	6.69×10^{-3}	2.57×10^{5}	8.47×10^{5}	7.33	24.10	3.29
HEXVEM	28.43	15.94	0.90	3.57×10^{-4}	6.68×10^{-3}	3.02×10^{5}	9.05×10^{5}	6.23	18.69	3.00
SAPBIW	28.19	23.24	0.88	4.65×10^{-4}	9.13×10^{-3}	3.92×10^{5}	1.16×10^{6}	6.65	19.63	2.95
RUTNOK	25.05	12.95	0.88	2.63×10^{-4}	5.81×10^{-3}	2.73×10^{5}	7.94×10^{5}	7.60	22.06	2.90
MOVPEU	16.16	14.92	0.77	7.10×10^{-5}	5.92×10^{-3}	2.19×10^{5}	6.30×10^{5}	28.95	83.23	2.87
BOGFIM	10.54	9.08	0.82	1.08×10^{-4}	4.03×10^{-3}	1.65×10^{5}	4.62×10^{5}	13.29	37.27	2.80
SOVGUF	7.99	7.06	0.79	8.36×10^{-4}	1.15×10^{-2}	5.00×10^{5}	1.26×10^{6}	5.44	13.75	2.53
RUBDUP	21.11	19.25	0.87	3.80×10^{-4}	6.94×10^{-3}	3.71×10^{5}	9.13×10^{5}	7.43	18.27	2.46
XANLEF	22.31	11.71	0.85	2.45×10^{-4}	4.03×10^{-3}	2.13×10^{5}	5.12×10^{5}	6.86	16.49	2.40
IZOWAW	18.36	8.13	0.76	2.29×10^{-4}	2.94×10^{-3}	1.21×10^{5}	2.87×10^{5}	5.39	12.80	2.38
TOVKOG	22.84	13.13	0.86	1.71×10^{-4}	5.11×10^{-3}	3.05×10^{5}	7.17×10^{5}	12.74	29.96	2.35
GESVAC	16.01	11.92	0.82	2.27×10^{-4}	3.64×10^{-3}	1.81×10^{5}	4.14×10^{5}	6.99	16.02	2.29
TOCJAY	24.08	19.56	0.85	3.42×10^{-4}	6.40×10^{-3}	3.56×10^{5}	8.08×10^{5}	8.23	18.69	2.27

[a]This list consists of MOFs with $S^0_{mem,H_2/CO_2} > 2.27$ and $P^0_{H_2} > 10^5$ Barrer. MOFs are ranked based on $S^0_{mem,H_2/CO_2}$.

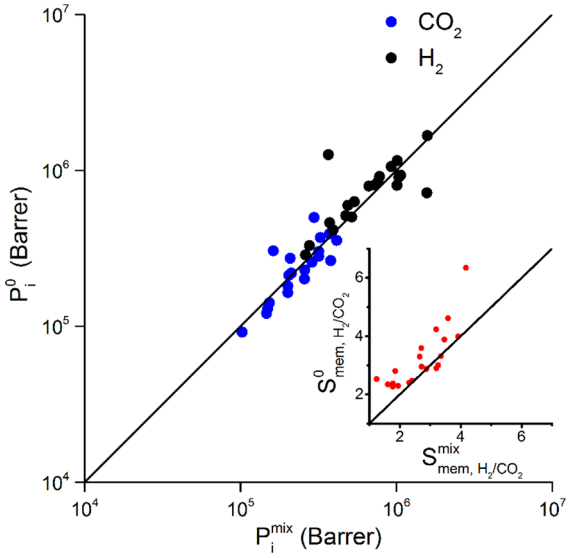


Figure 6. Comparison of gas permeabilities computed at infinite dilution ($P^0_{H_2}$ and $P^0_{CO_2}$) with the permeabilities computed for CO_2/H_2:15/85 binary mixture ($P^{mix}_{H_2}$ and $P^{mix}_{CO_2}$). (Inset) Comparison of the selectivities computed at infinite dilution, $S^0_{mem,H_2/CO_2}$, with the mixture selectivities, $S^{mix}_{mem,H_2/CO_2}$.

S3. $S^0_{mem,CO_2/H_2}$ and $P^0_{CO_2}$ were calculated to be in the range of 1.50×10^{-1} −4.25×10^3 and 1.85×10^4−6.71×10^8 Barrer, respectively. Blue points in Figure S3 show the 172 MOFs having CO_2 permeabilities greater than 10^7 Barrer, whereas the red points represent the top CO_2-selective membranes, offering CO_2/H_2 selectivity > 400 and $P^0_{CO_2} > 10^7$ Barrer. Table S3 lists these top MOFs, which are potential candidates as reverse selective membranes. The most CO_2-selective MOF was HESJOE, and its high membrane selectivity can be explained with the very high adsorption selectivity for CO_2 over H_2 due to its low porosity (0.51) and narrow pore size (4.74 Å). The second most promising MOF membrane was identified as KAXQOR, for which an experimental study reported a high heat of adsorption for CO_2 due to the ionic nature of Ca−O bonding in the framework,[76] which supports the high CO_2 selectivity we predicted. Although it was recently discussed that fabricating reproductive reverse selective porous membranes is a challenging issue,[73] our results suggest that there is a strong potential for this application of MOF membranes. Finally, we would like to note that we only considered selectivity and permeability in defining the most promising membrane materials. The judicious selection of the best membranes should also consider easiness in synthesis as well as long-term stability, which are more likely to be addressed by experimental studies.

3.3. Structure−Performance Relation Analyses. We finally examined structure−performance relations of MOF adsorbents and membranes. Figure 7a shows the relation between porosity, LCD, and adsorption selectivity of MOFs computed at infinite dilution. As the size of the bubbles increases, adsorption selectivities also increase. Due to the stronger confinement of CO_2 molecules in the narrow pores, MOFs with low LCDs (4.51−10.43 Å) and low porosities (0.36−0.65) are the adsorbents showing high CO_2/H_2 selectivities (>10 000). On the other hand, MOFs that have large pore sizes (>15 Å) and high porosities (>0.8) generally have low adsorption selectivities, <100, since both gas molecules are easily adsorbed. Similar structure−performance relations for membranes are shown in Figure 7b. MOFs with large LCDs and high porosities become H_2-selective membranes. Most of the promising H_2-selective MOF membranes are located in the region of 15 < LCD < 35 Å and 0.7 < ϕ < 1 in Figure 7b. As the pore sizes and porosities increase, CO_2 adsorption selectivities decrease as shown in Figure 7a and diffusion selectivities toward H_2 compensate for the low adsorption selectivities toward CO_2 in the large-pored materials. As a result, large-pored MOFs become H_2-selective membranes. In contrast, MOFs having narrow pores (<7.5 Å) and small porosities (<0.6) shown by red colors become the

DOI: 10.1021/acsami.8b12746
ACS Appl. Mater. Interfaces 2018, 10, 33693−33706

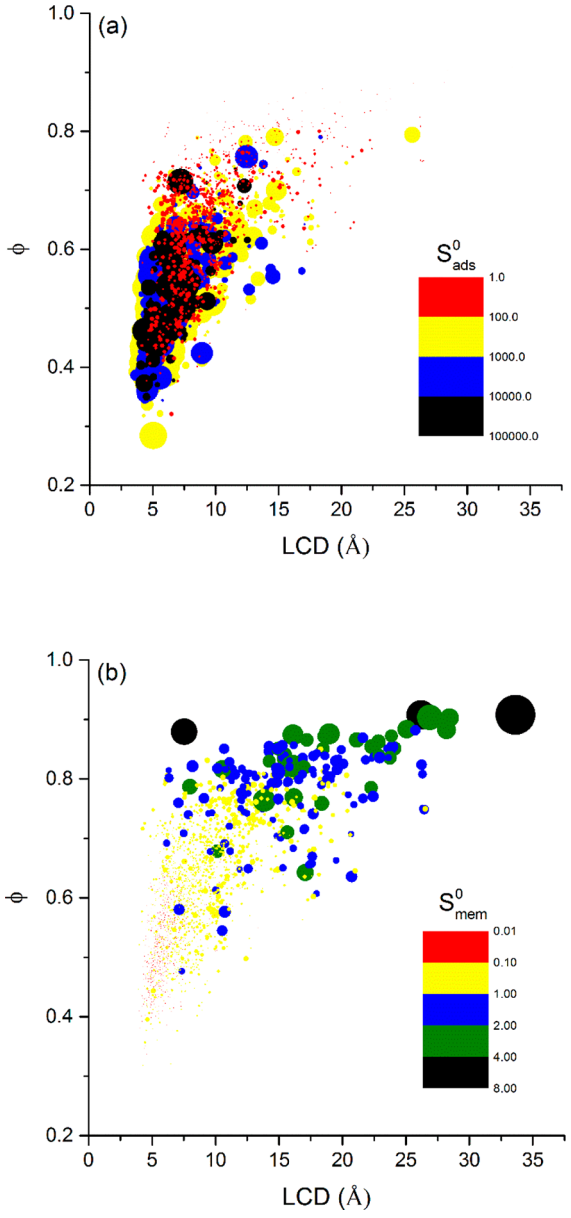


Figure 7. (a) Relation between porosities, pore sizes, and CO_2/H_2 adsorption selectivities of MOFs. (b) Relation between porosities, pore sizes, and H_2/CO_2 membrane selectivities of MOFs. Size of the bubbles represents selectivities of MOFs. Red, yellow, blue, and black regions were scaled with a factor of 4.0×10^{-2}, 2.4×10^{-2}, 2.4×10^{-3}, and 2.4×10^{-4}, respectively in a; scaling factor of 5 was used in b to have a clear representation.

CO_2-selective (reverse selective) MOF membranes as also presented in Table S3.

Detailed investigation of the structure−performance relationship for the top promising MOFs identified for PSA, VSA, and H_2-selective membrane-based gas separation applications can provide better understanding for future experimental studies. We analyzed the effects of each structural property, namely, PLD, LCD, SA, ϕ, and metal type, on the performance of the top MOF adsorbents and membranes in Figure 8. The main trend observed for PLD and LCD in Figure 7 is also seen for the top MOFs in Figure 8. Materials with narrow pores are better adsorbents. Eighteen (20) of the top 20 MOFs for the PSA (VSA) process were found to have PLDs < 7.5 Å. Similarly, 13 (19) of the top 20 MOFs for the PSA (VSA) process were identified to have LCDs < 7.5 Å. On the other hand, 16 of the top 20 MOF membranes were shown to have PLDs (LCDs) > 10 (15) Å, supporting our previous discussion that highly promising MOF membranes generally have large pores. Figure 8 shows that top MOF adsorbents have low SAs (<2000 m^2/g), whereas the top MOF membranes have large SAs (>3000 m^2/g). Another interesting feature of Figure 8 is that all of the top MOF adsorbents for the PSA process have porosities between 0.5 and 0.75, whereas all of the top MOF membranes have high porosities, >0.75. These results highlight that choosing the type of separation process prior to material selection is essential since different structural characteristics are desired for adsorption and membrane-based CO_2/H_2 separations. We then examined the type of the metal available in the MOF, but a clear structure−performance relation was not observed for PSA and VSA processes, whereas most of the top MOF membranes have Zn as the metal type as shown in Figure 8.

The difference between the isosteric heats of adsorption of gas molecules computed at infinite dilution (ΔQ^0_{st}) cannot be accounted for as a direct structural property, but it can be a useful parameter to assess the affinity of a MOF structure toward a specific gas. ΔQ^0_{st} was high, $10 < \Delta Q^0_{st} < 20$ kJ/mol and $20 < \Delta Q^0_{st} < 30$ kJ/mol, for the top adsorbents of for PSA and VSA, respectively, whereas it was relatively low, $0 < \Delta Q^0_{st} < 20$ kJ/mol, for the top membranes. This is expected because if ΔQ^0_{st} is large for MOFs, the MOF is strongly adsorbing CO_2 over H_2 and becoming a CO_2-selective adsorbent and CO_2-selective membrane (hence a weakly H_2 selective membrane). We finally used similarity index calculations[21,77,78] to compare surface texture and topology of the top MOFs. Figure S4 illustrates the similarity analysis of the top 20 MOFs in each process, PSA, VSA, and membrane-based separation. A similarity index (SI) changes from 0 to 1, showing how the structure of MOF resembles among all of the top MOFs identified in this study. SI > 0.8 indicates the most similar materials, whereas SI < 0.3 shows the least similar structures. The average SIs computed for the MOF adsorbents for PSA and VSA were 0.68 and 0.74, respectively, and the average SI computed for the top H_2-selective membranes was 0.57. These results suggest that topological structures of promising MOF adsorbents and membranes are quite similar.

Our simulation results showed that MOF membranes show promising performance, which allows us to overcome the permeability/selectivity trade-off observed in polymeric membranes. At that point it is important to note that molecular simulations do not consider practical limitations such as grain-boundary defects and other difficulties in making perfect MOF membranes such as limited adhesion of the membrane to the support, poor crystal intergrowth, and poor reproducibility, which can affect the overall performance of the MOF membrane. Therefore, our computational results should be viewed as the optimistic performance expectations from MOF membranes.

Finally, it is important to note that although MOFs are very promising membrane materials for CO_2 separation, there are still practical challenges that impede future application of MOF membranes. Venna and Carreon[79] recently discussed that even if MOF crystals having remarkable separation performances are prepared in the powder form, the same materials may not be suitable for membrane preparation because of several reasons such as limited adhesion of the membrane to the support, poor

DOI: 10.1021/acsami.8b12746
ACS Appl. Mater. Interfaces 2018, 10, 33693−33706

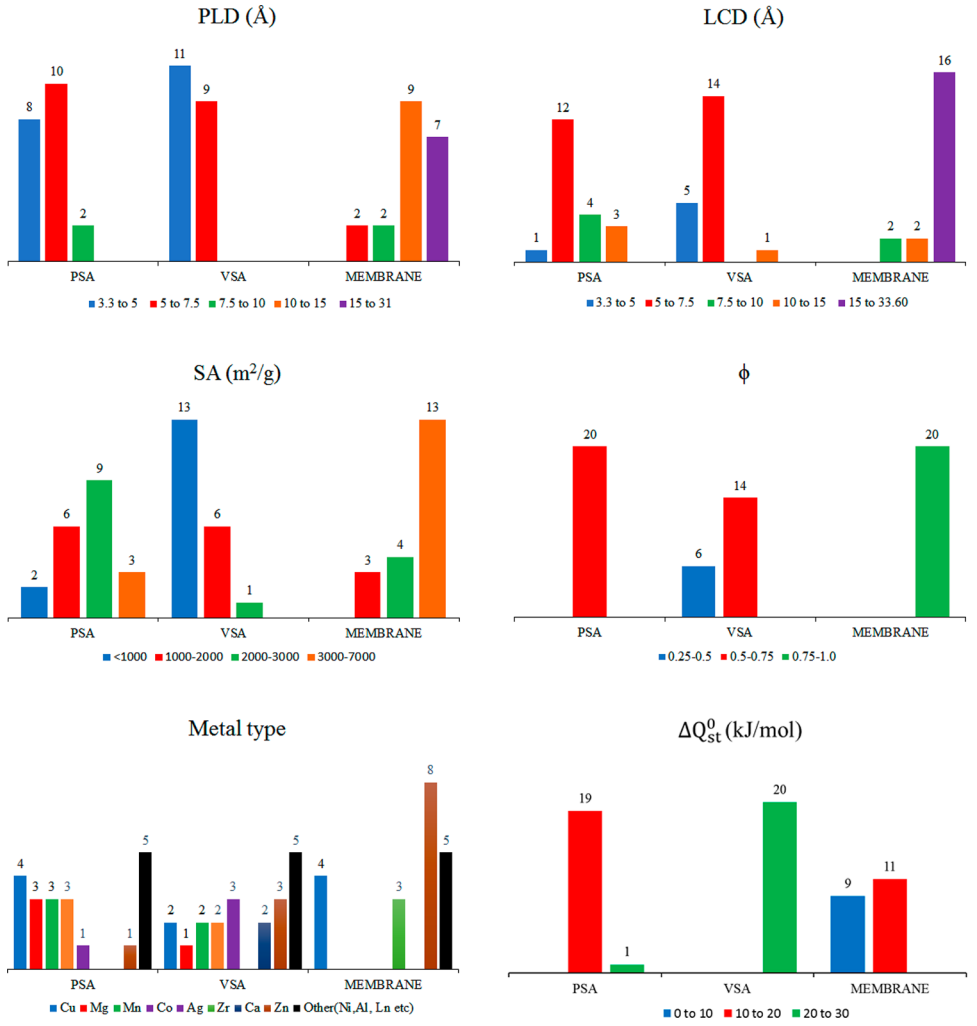


Figure 8. Effects of structural properties, PLD, LCD, SA, porosity, and metal type on the separation performances of the top 20 MOFs for PSA, VSA, and membrane processes.

crystal intergrowth, large crystal size resulting in non-continuous membranes, and poor reproducibility. Development of novel membrane synthesis methods, preparation of microporous crystals with small size and narrow size distribution for better crystal packing during membrane growth, seeding techniques to improve membrane intergrowth, and effective membrane−support interaction are suggested as the strategies that can lead to better MOF membranes having remarkable separation performances.

4. CONCLUSION

We performed a high-throughput computational screening study in order to define the best MOF adsorbents and membranes for CO_2/H_2 separation. Adsorption data of binary CO_2/H_2 mixtures in 3857 MOFs was obtained using GCMC simulations. Materials having $R\% > 85\%$ were ranked based on their APSs to identify the top 20 adsorbents for PSA and VSA processes. MD simulations were performed to compute permeabilities and selectivities of MOF membranes. A significant number of MOFs (899) exceeds the upper bound defined for polymeric membranes, suggesting that MOFs have the potential to replace traditional membranes in selective separation of H_2 from CO_2. Detailed examination of the structural characteristics of the top MOF adsorbents and membranes revealed that MOFs with pore sizes < 7.5 Å, $0.5 < \phi < 0.75$, and SA < 2000 m^2/g are good adsorbents, whereas the top MOF membranes have pore sizes > 15 Å, $\phi > 0.75$, and SA > 3000 m^2/g. These structure−performance relations will be useful to direct the experimental studies for the design and development of novel MOF materials that can achieve high-performance H_2/CO_2 separations.

■ ASSOCIATED CONTENT

Supporting Information

The Supporting Information is available free of charge on the ACS Publications website at DOI: 10.1021/acsami.8b12746.

Comparison of adsorption selectivities for CO_2/H_2:15/85 mixtures computed at infinite dilution, 0.1, 1, and 10 bar; comparison of experimentally measured and simulated CO_2 and H_2 isotherms of MOFs; figures representing separation performances of reverse selective membranes; structural similarity index comparisons of the top MOFs in PSA, VSA, and membrane-based separation processes; details of the experimental data for CO_2 and H_2 uptakes of MOFs, CO_2, and H_2 permeances of MOFs membranes; characteristic and separation properties of the top 20 reverse selective MOF membranes (PDF)

DOI: 10.1021/acsami.8b12746
ACS Appl. Mater. Interfaces 2018, 10, 33693−33706

AUTHOR INFORMATION

Corresponding Author

*E-mail: skeskin@ku.edu.tr. Phone: +90 (212) 338-1362.

ORCID

Seda Keskin: 0000-0001-5968-0336

Notes

The authors declare no competing financial interest.

ACKNOWLEDGMENTS

S.K. acknowledges a ERC-2017-Starting Grant. This study received funding from the European Research Council (ERC) under the European Union's Horizon 2020 research and innovation programme (ERC-2017-Starting Grant, grant agreement no. 756489-COSMOS).

REFERENCES

(1) Kenarsari, S. D.; Yang, D.; Jiang, G.; Zhang, S.; Wang, J.; Russell, A. G.; Wei, Q.; Fan, M. Review of recent advances in carbon dioxide separation and capture. *RSC Adv.* **2013**, *3* (45), 22739−22773.

(2) Yu, J.; Xie, L.-H.; Li, J.-R.; Ma, Y.; Seminario, J. M.; Balbuena, P. B. CO_2 capture and separations using MOFs: computational and experimental studies. *Chem. Rev.* **2017**, *117* (14), 9674−9754.

(3) Yampolskii, Y. Polymeric gas separation membranes. *Macromolecules* **2012**, *45* (8), 3298−3311.

(4) Sanders, D. F.; Smith, Z. P.; Guo, R.; Robeson, L. M.; McGrath, J. E.; Paul, D. R.; Freeman, B. D. Energy-efficient polymeric gas separation membranes for a sustainable future: A review. *Polymer* **2013**, *54* (18), 4729−4761.

(5) Korelskiy, D.; Ye, P.; Fouladvand, S.; Karimi, S.; Sjöberg, E.; Hedlund, J. Efficient ceramic zeolite membranes for CO_2/H_2 separation. *J. Mater. Chem. A* **2015**, *3* (23), 12500−12506.

(6) Li, H.; Haas-Santo, K.; Schygulla, U.; Dittmeyer, R. Inorganic microporous membranes for H_2 and CO_2 separation-Review of experimental and modeling progress. *Chem. Eng. Sci.* **2015**, *127*, 401−417.

(7) Li, J.-R.; Sculley, J.; Zhou, H.-C. Metal−organic frameworks for separations. *Chem. Rev.* **2012**, *112* (2), 869−932.

(8) Chen, T.-H.; Popov, I.; Kaveevivitchai, W.; Miljanić, O. Š. Metal−Organic Frameworks: Rise of the Ligands. *Chem. Mater.* **2014**, *26* (15), 4322−4325.

(9) Li, H.; Wang, K.; Sun, Y.; Lollar, C. T.; Li, J.; Zhou, H.-C. Recent advances in gas storage and separation using metal−organic frameworks. *Mater. Today* **2018**, *21* (2), 108−121.

(10) Erucar, I.; Keskin, S. Computational investigation of metal organic frameworks for storage and delivery of anticancer drugs. *J. Mater. Chem. B* **2017**, *5* (35), 7342−7351.

(11) Lee, J.; Farha, O. K.; Roberts, J.; Scheidt, K. A.; Nguyen, S. T.; Hupp, J. T. Metal−organic framework materials as catalysts. *Chem. Soc. Rev.* **2009**, *38* (5), 1450−1459.

(12) Belmabkhout, Y.; Guillerm, V.; Eddaoudi, M. Low concentration CO_2 capture using physical adsorbents: Are metal−organic frameworks becoming the new benchmark materials? *Chem. Eng. J.* **2016**, *296*, 386−397.

(13) Keskin, S.; Van Heest, T. M.; Sholl, D. S. Can metal-organic framework materials play a useful role in large-scale carbon dioxide separations? *ChemSusChem* **2010**, *3* (8), 879−891.

(14) Li, J.-R.; Ma, Y.; McCarthy, M. C.; Sculley, J.; Yu, J.; Jeong, H.-K.; Balbuena, P. B.; Zhou, H.-C. Carbon dioxide capture-related gas adsorption and separation in metal-organic frameworks. *Coord. Chem. Rev.* **2011**, *255* (15), 1791−1823.

(15) Qiu, S.; Xue, M.; Zhu, G. Metalorganic framework membranes: from synthesis to separation application. *Chem. Soc. Rev.* **2014**, *43* (16), 6116−6140.

(16) Herm, Z. R.; Swisher, J. A.; Smit, B.; Krishna, R.; Long, J. R. Metal-organic frameworks as adsorbents for hydrogen purification and precombustion carbon dioxide capture. *J. Am. Chem. Soc.* **2011**, *133* (15), 5664−5667.

(17) Nandi, S.; De Luna, P.; Daff, T. D.; Rother, J.; Liu, M.; Buchanan, W.; Hawari, A. I.; Woo, T. K.; Vaidhyanathan, R. A single-ligand ultra-microporous MOF for precombustion CO_2 capture and hydrogen purification. *Sci. Adv.* **2015**, *1* (11), e1500421.

(18) Qiao, Z. W.; Zhang, K.; Jiang, J. W. In Silico Screening of 4764 Computation-Ready, Experimental Metal-Organic Frameworks for CO_2 Separation. *J. Mater. Chem. A* **2016**, *4* (6), 2105−2114.

(19) Wu, D.; Yang, Q. Y.; Zhong, C. L.; Liu, D. H.; Huang, H. L.; Zhang, W. J.; Maurin, G. Revealing the structure-property relationships of metal-organic frameworks for CO_2 capture from flue gas. *Langmuir* **2012**, *28* (33), 12094−12099.

(20) Haldoupis, E.; Nair, S.; Sholl, D. S. Finding MOFs for highly selective CO_2/N_2 adsorption using materials screening based on efficient assignment of atomic point charges. *J. Am. Chem. Soc.* **2012**, *134* (9), 4313−4323.

(21) Altintas, C.; Avci, G.; Daglar, H.; Gulcay, E.; Erucar, I.; Keskin, S. Computer simulations of 4240 MOF membranes for H_2/CH_4 separations: insights into structure−performance relations. *J. Mater. Chem. A* **2018**, *6* (14), 5836−5847.

(22) Qiao, Z.; Wang, N.; Jiang, J.; Zhou, J. Design of amine-functionalized metal−organic frameworks for CO 2 separation: the more amine, the better? *Chem. Commun.* **2016**, *52* (5), 974−977.

(23) Tong, M.; Yang, Q.; Zhong, C. Computational screening of covalent organic frameworks for CH_4/H_2, CO_2/H_2 and CO_2/CH_4 separations. *Microporous Mesoporous Mater.* **2015**, *210*, 142−148.

(24) Park, J.; Lively, R. P.; Sholl, D. S. Establishing upper bounds on CO_2 swing capacity in sub-ambient pressure swing adsorption via molecular simulation of metal−organic frameworks. *J. Mater. Chem. A* **2017**, *5* (24), 12258−12265.

(25) Chung, Y. G.; Gómez-Gualdrón, D. A.; Li, P.; Leperi, K. T.; Deria, P.; Zhang, H.; Vermeulen, N. A.; Stoddart, J. F.; You, F.; Hupp, J. T. In silico discovery of metal-organic frameworks for precombustion CO_2 capture using a genetic algorithm. *Science advances* **2016**, *2* (10), e1600909.

(26) Krishna, R.; van Baten, J. M. In silico screening of metal−organic frameworks in separation applications. *Phys. Chem. Chem. Phys.* **2011**, *13* (22), 10593−10616.

(27) Moghadam, P. Z.; Li, A.; Wiggin, S. B.; Tao, A.; Maloney, A. G. P.; Wood, P. A.; Ward, S. C.; Fairen-Jimenez, D. Development of a cambridge structural database subset: A collection of metal−organic frameworks for past, present, and future. *Chem. Mater.* **2017**, *29* (7), 2618−2625.

(28) Allen, F. H. The Cambridge structural database: A quarter of a million crystal structures and rising. *Acta Crystallogr., Sect. B: Struct. Sci.* **2002**, *58*, 380−388.

(29) Willems, T. F.; Rycroft, C. H.; Kazi, M.; Meza, J. C.; Haranczyk, M. Algorithms and tools for high-throughput geometry-based analysis of crystalline porous materials. *Microporous Mesoporous Mater.* **2012**, *149* (1), 134−141.

(30) Walton, K. S.; Snurr, R. Q. Applicability of the BET method for determining surface areas of microporous metal−organic frameworks. *J. Am. Chem. Soc.* **2007**, *129* (27), 8552−8556.

(31) Koyuturk, B.; Altintas, C.; Kinik, F. P.; Keskin, S.; Uzun, A. Improving gas separation performance of ZIF-8 by [BMIM][BF4] incorporation: Interactions and their consequences on performance. *J. Phys. Chem. C* **2017**, *121* (19), 10370−10381.

(32) Dubbeldam, D.; Calero, S.; Ellis, D. E.; Snurr, R. Q. RASPA: Molecular simulation software for adsorption and diffusion in flexible nanoporous materials. *Mol. Simul.* **2016**, *42* (2), 81−101.

(33) Rappe, A. K.; Casewit, C. J.; Colwell, K. S.; Goddard, W. A., III; Skiff, W. M. UFF, a full periodic table force field for molecular mechanics and molecular dynamics simulations. (Universal force field). *J. Am. Chem. Soc.* **1992**, *114* (25), 10024−10035.

(34) Sumer, Z.; Keskin, S. Ranking of MOF adsorbents for CO_2 Separations: A molecular simulation study. *Ind. Eng. Chem. Res.* **2016**, *55* (39), 10404−10419.

DOI: 10.1021/acsami.8b12746
ACS Appl. Mater. Interfaces 2018, 10, 33693−33706

(35) Adatoz, E.; Keskin, S. Application of MD simulations to predict membrane properties of MOFs. *J. Nanomater.* **2015**, *2015*, 1.
(36) Basdogan, Y.; Keskin, S. Simulation and modelling of MOFs for hydrogen storage. *CrystEngComm* **2015**, *17* (2), 261−275.
(37) Altintas, C.; Erucar, I.; Keskin, S. High-throughput computational screening of the metal organic framework database for CH_4/H_2 separations. *ACS Appl. Mater. Interfaces* **2018**, *10* (4), 3668−3679.
(38) Ozturk, T. N.; Keskin, S. Predicting gas separation performances of porous coordination networks using atomistic simulations. *Ind. Eng. Chem. Res.* **2013**, *52* (49), 17627−17639.
(39) Erucar, I.; Manz, T. A.; Keskin, S. Effects of electrostatic interactions on gas adsorption and permeability of MOF membranes. *Mol. Simul.* **2014**, *40* (7−9), 557−570.
(40) Erucar, I.; Keskin, S. Computational modeling of bio-MOFs for CO_2/CH_4 separations. *Chem. Eng. Sci.* **2015**, *130*, 120−128.
(41) Buch, V. Path integral simulations of mixed para -D_2 and ortho -D_2 clusters: The orientational effects. *J. Chem. Phys.* **1994**, *100* (10), 7610−7629.
(42) Potoff, J. J.; Siepmann, J. I. Vapor−liquid equilibria of mixtures containing alkanes, carbon dioxide, and nitrogen. *AIChE J.* **2001**, *47* (7), 1676−1682.
(43) Piper, J.; Morrison, J.; Peters, C. The adsorption of carbon monoxide on graphite. *Mol. Phys.* **1984**, *53* (6), 1463−1480.
(44) Martin, M. G.; Siepmann, J. I. Transferable potentials for phase equilibria. 1. United-atom description of n-alkanes. *J. Phys. Chem. B* **1998**, *102* (14), 2569−2577.
(45) Jorgensen, W. L.; Chandrasekhar, J.; Madura, J. D.; Impey, R. W.; Klein, M. L. Comparison of simple potential functions for simulating liquid water. *J. Chem. Phys.* **1983**, *79* (2), 926−935.
(46) Ewald, P. P. Die Berechnung optischer und elektrostatischer Gitterpotentiale. *Ann. Phys.* **1921**, *369* (3), 253−287.
(47) Evans, D. J.; Holian, B. L. The nose−hoover thermostat. *J. Chem. Phys.* **1985**, *83* (8), 4069−4074.
(48) Erucar, I.; Keskin, S. Computational assessment of MOF membranes for CH_4/H_2 separations. *J. Membr. Sci.* **2016**, *514*, 313−321.
(49) Oreggioni, G. D.; Brandani, S.; Luberti, M.; Baykan, Y.; Friedrich, D.; Ahn, H. CO_2 capture from syngas by an adsorption process at a biomass gasification CHP plant: Its comparison with amine-based CO_2 capture. *Int. J. Greenhouse Gas Control* **2015**, *35*, 71−81.
(50) Hufton, J.; Mayorga, S.; Sircar, S. Sorption-enhanced reaction process for hydrogen production. *AIChE J.* **1999**, *45* (2), 248−256.
(51) Krishna, R. Screening metal−organic frameworks for mixture separations in fixed-bed adsorbers using a combined selectivity/capacity metric. *RSC Adv.* **2017**, *7* (57), 35724−35737.
(52) Bae, Y. S.; Snurr, R. Q. Development and evaluation of porous materials for carbon dioxide separation and capture. *Angew. Chem., Int. Ed.* **2011**, *50* (49), 11586−11596.
(53) Fang, H.; Kulkarni, A.; Kamakoti, P.; Awati, R.; Ravikovitch, P. I.; Sholl, D. S. Identification of high-CO_2-capacity cationic zeolites by accurate computational screening. *Chem. Mater.* **2016**, *28* (11), 3887−3896.
(54) Krishna, R. Methodologies for screening and selection of crystalline microporous materials in mixture separations. *Sep. Purif. Technol.* **2018**, *194*, 281−300.
(55) Dantas, T. L.; Luna, F. M. T.; Silva, I. J., Jr; Torres, A. E. B.; de Azevedo, D. C.; Rodrigues, A. E.; Moreira, R. F. Carbon dioxide−nitrogen separation through pressure swing adsorption. *Chem. Eng. J.* **2011**, *172* (2−3), 698−704.
(56) Shirani, B.; Eic, M. Novel differential column method for measuring multicomponent gas adsorption isotherms in NaY zeolite. *Ind. Eng. Chem. Res.* **2017**, *56* (4), 1008−1018.
(57) Hefti, M.; Marx, D.; Joss, L.; Mazzotti, M. Adsorption equilibrium of binary mixtures of carbon dioxide and nitrogen on zeolites ZSM-5 and 13X. *Microporous Mesoporous Mater.* **2015**, *215*, 215−228.
(58) Lässig, D.; Lincke, J.; Moellmer, J.; Reichenbach, C.; Moeller, A.; Gläser, R.; Kalies, G.; Cychosz, K. A.; Thommes, M.; Staudt, R. A microporous copper metal−organic framework with high H_2 and CO_2 adsorption capacity at ambient pressure. *Angew. Chem., Int. Ed.* **2011**, *50* (44), 10344−10348.
(59) Qian, J.; Jiang, F.; Yuan, D.; Wu, M.; Zhang, S.; Zhang, L.; Hong, M. Highly selective carbon dioxide adsorption in a water-stable indium−organic framework material. *Chem. Commun.* **2012**, *48* (78), 9696−9698.
(60) Huang, H.; Zhang, W.; Liu, D.; Zhong, C. Understanding the effect of trace amount of water on CO_2 capture in natural gas upgrading in metal−organic frameworks: A molecular simulation study. *Ind. Eng. Chem. Res.* **2012**, *51* (30), 10031−10038.
(61) Liu, B.; Smit, B. Comparative molecular simulation study of CO_2/N_2 and CH_4/N_2 separation in zeolites and metal−organic frameworks. *Langmuir* **2009**, *25* (10), 5918−5926.
(62) Babarao, R.; Jiang, J. Upgrade of natural gas in rho zeolite-like metal−organic framework and effect of water: A computational study. *Energy Environ. Sci.* **2009**, *2* (10), 1088−1093.
(63) Mason, J. A.; McDonald, T. M.; Bae, T.-H.; Bachman, J. E.; Sumida, K.; Dutton, J. J.; Kaye, S. S.; Long, J. R. Application of a high-throughput analyzer in evaluating solid adsorbents for post-combustion carbon capture via multicomponent adsorption of CO_2, N_2, and H_2O. *J. Am. Chem. Soc.* **2015**, *137* (14), 4787−4803.
(64) Li, J.; Li, P.-Z.; Li, Q.-Y.; Cao, Y.; Lu, H.; Wu, H.; Li, F.; Shi, Y.; Wang, X.-J.; Zhao, Y. An rht-type metal−organic framework constructed from an unsymmetrical ligand exhibiting high hydrogen uptake capability. *RSC Adv.* **2014**, *4* (96), 53975−53980.
(65) Robeson, L. M. The upper bound revisited. *J. Membr. Sci.* **2008**, *320* (1−2), 390−400.
(66) Li, Y.; Liang, F.; Bux, H.; Yang, W.; Caro, J. Zeolitic imidazolate framework ZIF-7 based molecular sieve membrane for hydrogen separation. *J. Membr. Sci.* **2010**, *354* (1−2), 48−54.
(67) Qiu, S.; Xue, M.; Zhu, G. Metal−organic framework membranes: from synthesis to separation application. *Chem. Soc. Rev.* **2014**, *43* (16), 6116−6140.
(68) Fan, L.; Xue, M.; Kang, Z.; Li, H.; Qiu, S. Electrospinning technology applied in zeolitic imidazolate framework membrane synthesis. *J. Mater. Chem.* **2012**, *22* (48), 25272−25276.
(69) Zhang, X.; Liu, Y.; Li, S.; Kong, L.; Liu, H.; Li, Y.; Han, W.; Yeung, K. L.; Zhu, W.; Yang, W.; Qiu, J. New membrane architecture with high performance: ZIF-8 membrane supported on vertically aligned ZnO nanorods for gas permeation and separation. *Chem. Mater.* **2014**, *26* (5), 1975−1981.
(70) Feng, D.; Wang, K.; Su, J.; Liu, T. F.; Park, J.; Wei, Z.; Bosch, M.; Yakovenko, A.; Zou, X.; Zhou, H. C. A highly stable zeotype mesoporous zirconium metal−organic framework with ultralarge pores. *Angew. Chem., Int. Ed.* **2015**, *54* (1), 149−154.
(71) Oisaki, K.; Li, Q.; Furukawa, H.; Czaja, A. U.; Yaghi, O. M. A Metal−organic framework with covalently bound organometallic complexes. *J. Am. Chem. Soc.* **2010**, *132* (27), 9262−9264.
(72) Feng, D.; Wang, K.; Wei, Z.; Chen, Y.-P.; Simon, C. M.; Arvapally, R. K.; Martin, R. L.; Bosch, M.; Liu, T.-F.; Fordham, S. Kinetically tuned dimensional augmentation as a versatile synthetic route towards robust metal−organic frameworks. *Nat. Commun.* **2014**, *5*, 5723.
(73) Li, P.; Wang, Z.; Qiao, Z.; Liu, Y.; Cao, X.; Li, W.; Wang, J.; Wang, S. Recent developments in membranes for efficient hydrogen purification. *J. Membr. Sci.* **2015**, *495*, 130−168.
(74) Zhao, Z.; Ma, X.; Kasik, A.; Li, Z.; Lin, Y. Gas separation properties of metal organic framework (MOF-5) membranes. *Ind. Eng. Chem. Res.* **2013**, *52* (3), 1102−1108.
(75) Freeman, B. D. Basis of permeability/selectivity tradeoff relations in polymeric gas separation membranes. *Macromolecules* **1999**, *32* (2), 375−380.
(76) Banerjee, D.; Zhang, Z.; Plonka, A. M.; Li, J.; Parise, J. B. A calcium coordination framework having permanent porosity and high CO_2/N_2 selectivity. *Cryst. Growth Des.* **2012**, *12* (5), 2162−2165.
(77) Martin, R. L.; Smit, B.; Haranczyk, M. Addressing challenges of identifying geometrically diverse sets of crystalline porous materials. *J. Chem. Inf. Model.* **2012**, *52* (2), 308−318.

DOI: 10.1021/acsami.8b12746
ACS Appl. Mater. Interfaces 2018, 10, 33693−33706

(78) Pinheiro, M.; Martin, R. L.; Rycroft, C. H.; Jones, A.; Iglesia, E.; Haranczyk, M. Characterization and comparison of pore landscapes in crystalline porous materials. *J. Mol. Graphics Modell.* **2013**, *44*, 208−219.
(79) Venna, S. R.; Carreon, M. A. Metal organic framework membranes for carbon dioxide separation. *Chem. Eng. Sci.* **2015**, *124*, 3−19.

DOI: 10.1021/acsami.8b12746
ACS Appl. Mater. Interfaces 2018, 10, 33693−33706